# Role of clouds and land-atmosphere coupling in midlatitude continental summer warm biases and climate change amplification in CMIP5 simulations

F Cheruy, Jl Dufresne, F Hourdin, Agnès Ducharne

AGU PUBLICATIONS

Geophysical Research Letters

RESEARCH LETTER
10.1002/2014GL061145

**Key Points:**
- Systematic summer warm biases in regions of strong soil-atmosphere coupling
- Most biased models underestimate evaporative fraction and clouds
- Most biased models show a stronger warming in climate change projections

**Supporting Information:**
- Readme
- Table S1
- Table S2
- Figure S1

**Correspondence to:**
F. Cheruy,
cheruy@lmd.jussieu.fr

**Citation:**
Cheruy, F., J. L. Dufresne, F. Hourdin, and A. Ducharne (2014), Role of clouds and land-atmosphere coupling in midlatitude continental summer warm biases and climate change amplification in CMIP5 simulations, *Geophys. Res. Lett.*, *41*, 6493–6500, doi:10.1002/2014GL061145.

Received 7 JUL 2014
Accepted 25 AUG 2014
Accepted article online 27 AUG 2014
Published online 18 SEP 2014

# Role of clouds and land-atmosphere coupling in midlatitude continental summer warm biases and climate change amplification in CMIP5 simulations

**F. Cheruy[1], J. L. Dufresne[1], F. Hourdin[1], and A. Ducharne[2]**

[1]CNRS/IPSL/LMD, Université Pierre et Marie Curie, Paris, France, [2]UMR METIS, CNRS/UPMC, Paris, France

**Abstract** Over land, most state-of-the-art climate models contributing to Coupled Model Intercomparison Project Phase 5 (CMIP5) share a strong summertime warm bias in midlatitude areas, especially in regions where the coupling between soil moisture and atmosphere is effective. The most biased models overestimate solar incoming radiation, because of cloud deficit and have difficulty to sustain evaporation. These deficiencies are also involved in the spread of the summer temperature projections among models in the midlatitude; the models which simulate a higher-than-average warming overestimate the present climate net shortwave radiation which increases more-than-average in the future, in link with a decrease of cloudiness. They also show a higher-than-average reduction of evaporative fraction in areas with soil moisture-limited evaporation regimes. Over these areas, the most biased models in the present climate simulate a larger warming in response to climate change which is likely to be overestimated.

## 1. Introduction

Most state-of-the-art climate models from the Coupled Model Intercomparison Project (CMIP) tend to overpredict the summer near-surface temperature at midlatitudes [*Christensen and Boberg*, 2012; *Mueller and Seneviratne*, 2014]. It is the case for Regional Climate Model as well [*Boberg and Christensen*, 2012; *Vautard et al.*, 2013]. Biases in the present-day simulations cast doubts on the reliability of the future climate projections, and question the use of near-surface variables produced by numerical climate models for climate change impact studies. Various authors tackled this highly relevant topic but the discussion is still open; as an example, *Boberg and Christensen* [2012] argued that, in links with the warm bias in the present-day simulations, regional warming can be overestimated by as much as 10–30% over some regions but *Giorgi and Coppola* [2010] and *Coppola et al.* [2014] ended this much more balanced conclusion: "For temperature, the model regional bias has a negligible effect on the projected regional change." This context motivates the present study, which aims at better understanding the origin of these biases in the present-day simulations, and the dispersion in climate change projections.

Although it is generally agreed that the soil moisture-temperature feedback is crucial to assess the model deficiencies [e.g., *Jaeger and Seneviratne*, 2011], it remains difficult to precisely identify their causes, and to improve on them, because of the complexity of the processes involved in this feedback and the probable interplay between the general circulation and regional characteristics [e.g., *Boé*, 2013]. *Coindreau et al.* [2007] and *Cheruy et al.* [2013] showed how the summer biases in near-surface state variables simulated by the Institut Pierre-Simon Laplace Climate Model (IPSL-CM) are first explained by the sensible/latent heat partitioning, then by the radiative impact of clouds at the surface and the parameterization of turbulent transport in the surface layer. *Boé and Terray* [2008] pointed out large uncertainties in evapotranspiration changes in the CMIP Phase 3 models over Europe and possible feedback on the temperature change. These studies suggest that the way the surface energy balance is achieved in climate models is important for further understanding their spread in near-surface temperature.

In this paper, we adopt a multimodel approach, in an attempt to identify statistically robust relationships between various temperature and surface energy budget indices. We mostly rely on linear multimodel regressions, based on a multimodel ensemble from the CMIP Phase 5 (CMIP5) database [*Taylor et al.*, 2012]. The selected data and indices are detailed in section 2. Section 3 shows the resulting multimodel biases, and the regional correlations between temperature and energy budget indices. Section 4 discusses the impact

**Table 1.** Operators Used in the Analysis[a]

| Variable | Name | Expression |
|---|---|---|
| Observed value | $O_{i,j}$ | |
| Model value | $X_{i,j}(m,\text{exp})$ | |
| Bias | $X^b_{i,j}(m,\text{exp})$ | $X_{i,j}(m,\text{exp}) - O_{i,j}$ |
| Global mean, over the globe | $X_g(m,\text{exp})$ | $\frac{1}{A}\int X_{i,j}(m,\text{exp})dA$ |
| Multimodel mean | $\bar{X}_{i,j}(\text{exp})$ | $\sum_m X_{i,j}(m,\text{exp})/N$ |
| Intermodel anomaly | $X^a_{i,j}(m,\text{exp})$ | $X_{i,j}(m,\text{exp}) - \bar{X}_{i,j}(\text{exp})$ |
| Local anomaly | $X^l_{i,j}(m,\text{exp})$ | $X_{i,j}(m,\text{exp}) - X_g(m,\text{exp})$ |
| Response of $X$ to climate change | $\delta X_{i,j}(m)$ | $X_{i,j}(m,\text{RCP8.5}) - X_{i,j}(m,\text{hist})$ |
| Local sensitivity to global warming | $S_X(m)$ | $\delta X_{i,j}(m)/\delta T_{i,j}(m)$ |

[a]Observations and model values refer to summer climatological means, $m$ denotes a particular model, $i,j$ a grid point, exp an experiment (historical, AMIP, or RCP8.5), $N$ the total number of models, $A$ the total area of the Earth, and $X$ a climate variable.

of the surface energy budget uncertainties on the spread of future temperature change. Conclusions are drawn in section 5.

## 2. Data

The number of models in our ensemble (list in the supporting information) is determined by the availability of the analyzed variables, presented below, in the CMIP5 database. We consider 30 coupled ocean-atmosphere models for their reconstruction of the twentieth century climate, the so-called "historical" simulations, and for their climate change simulations, all forced with Representative Concentration Pathway "RCP8.5" corresponding to the pathway with the highest greenhouse gas emission. Only 25 of them provide the moisture in upper portion of the soil column (SM), and 28 provide all the terms of the surface energy budget. We also analyze, for 23 models, the so-called AMIP (Atmospheric Model Intercomparison Project) simulations, in which sea surface temperatures (SSTs) and sea ice extents are prescribed from observations. In all cases, we apply to the model outputs a first-order conservative remapping and a land-sea mask on a common $2° \times 2°$ longitude-latitude grid. For all variables, boreal summer climatological means are computed from the June-July-August mean values over a 30 year long period: 1979–2008 for AMIP simulations, 1976–2005 for historical coupled simulations, and 2070–2099 for RCP8.5 coupled simulations. Only these summer climatological means are used below.

For the analysis of surface fluxes (all counted positively when they heat the surface), we selected three composite indices. The screening effect of clouds, which reduces the shortwave (SW) radiation reaching the surface, is quantified by the surface shortwave cloud radiative effect (SWCRE), a negative quantity, calculated as the difference between all-sky and clear-sky downward shortwave radiation at the surface. The evaporative fraction ($\text{EF} = H_L/(H_S + H_L)$) quantifies the partition between the latent and sensible heat fluxes (respectively, $H_L$ and $H_S$). The correlation between latent heat flux and soil moisture is classically used to characterize the land-atmosphere coupling [*Guo et al.*, 2006]. A positive correlation corresponds to a regime where evaporation is limited by the availability of soil moisture. In contrast, a negative correlation characterizes a regime where surface net radiation drives the evaporation, so that a larger evaporation (more negative latent heat flux) depletes the soil moisture. We use here the coupling index defined by *Dirmeyer* [2011]; *Dirmeyer et al.* [2013], which relies on the interannual correlation between the soil moisture and the upward latent heat flux (noted $\text{SM}_{M,y}$ and $-H_{L_{M,y}}$, for summer months $M$ of years $y$), multiplied by the interannual standard deviation of the latent heat flux, to highlight the areas where the variations of the latent heat flux are important. It can be expressed as follows: $C = -\sigma_{H'_{L_{M,y}}} \cdot \text{Cov}(\text{SM}'_{M,y} \cdot H'_{L_{M,y}})/\sigma_{\text{SM}'_{M,y}}\sigma_{H'_{L_{M,y}}}$ which can be written as $C = -\sum(\text{SM}'_{M,y} \cdot H'_{L_{M,y}})/\sqrt{(\sum(\text{SM}'_{M,y})^2)}$ as well, with $'$ referring to the interannual anomaly. Positive values correspond to regions where moisture is more limited than energy and thus where soil moisture supply is the principal control on latent heat flux. To analyze the possible links between the surface fluxes, the above defined indices, and near-surface temperature $T$, we use several operators, defined in Table 1. In particular, for each model $m$, we define the intermodel anomaly as the anomaly with respect to the multimodel mean, in both present and future climate, by analogy with interannual anomalies; the local anomalies

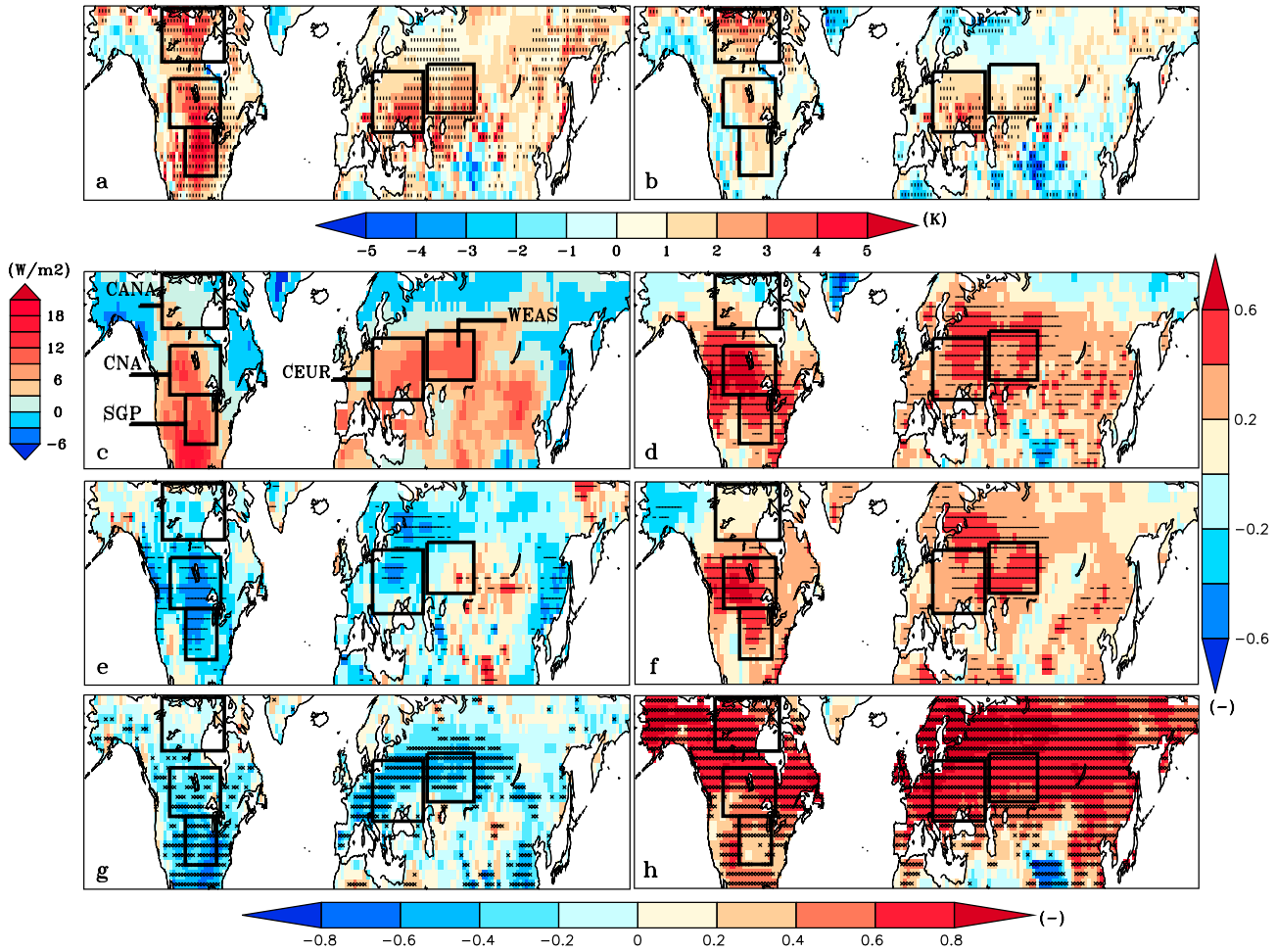


**Figure 1.** (a, b) Multimodel mean bias of summer temperature compared to CRU data (in K), for AMIP (Figure 1a) and historical (Figure 1b) simulations, with crosses in regions where at least 80% of the models agree on sign; (c) soil moisture-atmosphere coupling mean index $C$ (W m$^{-2}$); (d–f) correlation between local warming, $\delta T$, and bias of the historical values of temperature $T$ with respect to CRU (Figure 1d), historical values of EF (Figure 1e), SWCRE (Figure 1f) $\delta$EF (Figure 1g), and $\delta$SWCRE (Figure 1h), with horizontal bars or crosses in areas where the correlations are significant at the 90% level.

characterize the spatial departures from the global mean of model $m$, and filter out the global bias specific to each model; and finally the local sensitivity to global warming, $S_X(m)$, is the ratio of the local change in variable $X$ to the corresponding local warming and is computed from the RCP85 simulations.

We also use observations to document the model biases. Near-surface temperature from AMIP and historical simulations is compared to the 0.5° × 0.5° CRU-TS3.10 2 m temperature data set [*Mitchell and Jones*, 2005]. The Clouds and the Earth's Radiant Energy System Energy Balanced and Filled (CERES EBAF)-Surface 1° × 1° monthly product from 2000 to 2012 [*Kato et al.*, 2013] is used as a reference for the SW radiation. Estimations of monthly latent and sensible heat fluxes from 1982 to 2011 are taken from the 0.5° × 0.5° data set of *Jung et al.* [2011], based on the interpolation of FLUXNET data [*Baldocchi et al.*, 2001].

## 3. Bias and Spread in Current Climate Simulations

### 3.1. Near-Surface Temperature Biases

The AMIP simulation shows a quasi-systematic warm bias with respect to Climatic Research Unit (CRU) data in the northern midlatitude and high latitude (1a) with wide regions in which 80% of the models agree on the sign of the bias with a mean larger than 2 K. The mean bias in the historical experiments show a similar shape but with a reduced intensity (1b). We selected five regions where the AMIP multimodel mean bias is maximum (bounds given in the supporting information), namely Canada (CANA), Central North America (CNA), South Great Plains (SGP), Central Europe (CEUR), and Western Eurasian Steppes (WEAS). In the

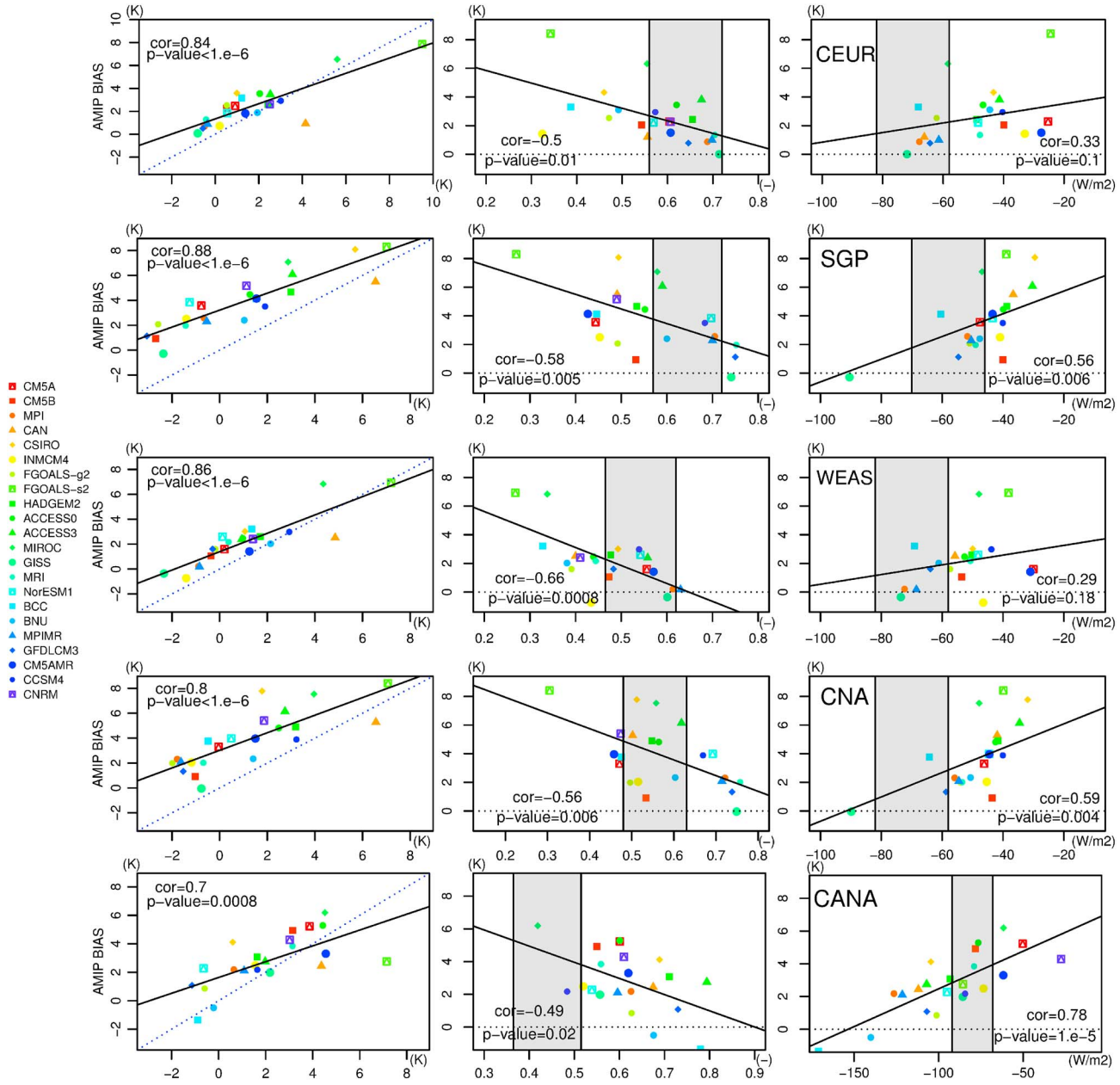


**Figure 2.** Bias of near-surface temperature in AMIP simulations (*y* axis), as a function of the bias in (left column) historical simulations, (middle column) EF, and (right column) SWCRE, on average over the five boxes. The dotted blue line in Figure 2 (left column) is the diagonal line. The grey-shaded area in Figures 2 (center column) and 2 (right column) are centered on the estimates from observations and shows the amplitude of the uncertainties estimated by *Jiménez et al.* [2011] for EF (from August zonal mean in Figure 11), and by *Kato et al.* [2013] for the SW radiation. The regression lines, the correlation coefficients, and the corresponding *p* values, are also displayed.

midlatitudes, thus excluding Canada, there is a good correspondence between these positively biased regions and areas with strong soil moisture-atmosphere coupling (Figure 1c).

As shown in Figure 2 (left), there is a strong correlation among models between the near-surface temperature bias ($X^b_{i,j}(m, \mathrm{exp})$) in the AMIP and historical experiments in the five regions. Coupling with ocean results in a systematic cooling, probably linked to error compensations or model tuning but the bias structure is not distorted. We can conclude that the model defects that lead to summer warm biases in forced SST simulations are also present in the coupled simulations. The link between the biases and the energy budget will then be analyzed based on AMIP simulations, which are not subject to SST biases while the climate change response will be addressed using the coupled ocean-atmosphere simulations.

### 3.2. Possible Sources of Near-Surface Temperature Spread

The relationships between the near-surface temperature bias and either EF or SWCRE are displayed in Figures 2 (center column) and 2 (right column) for the five regions. The uncertainties on the estimates of SWCRE and EF are large, but smaller than the simulations spread. The temperature bias is positive for almost all models, and the stronger the bias, the weaker SWCRE, and the smaller EF. In the four midlatitude regions (CEUR, SGP, CNA, and WEAS), compared to the CERES-EBAF estimates, most models underestimate the SW reflection by clouds, which may be interpreted as a lack of cloud cover. For CEUR, SGP, and WEAS, the evaporative fraction is underestimated by the models with the warmest bias. In Canada, in contrast, most models overestimate EF, while the less biased models exhibit a much too strong SWCRE.

In CEUR, SGP, and WEAS, the warm bias is associated with an underestimation of the evaporative fraction related to a deficit in soil moisture supply and with an overestimation of the net surface radiation related to a deficit of clouds. Both effects are typical of heat wave feedback loop: a warmer temperature reducing soil moisture and then evapotranspiration (for limited soil moisture regimes) and the clouds through the coupling with the boundary layer [*Fischer et al.*, 2007]. For the IPSL-CM model, in-depth analysis over Europe showed that this warm summer bias could be specifically attributed to deficiencies in the parameterization of soil hydrology and in the cloud scheme [*Cheruy et al.*, 2013; *Campoy et al.*, 2013]. In contrast, CNA can be considered as a transitional region: the surface net radiation is always overestimated but no systematic bias exists for EF, here soil moisture-limited regime is likely to be less frequent. For CANA where limited energy regime is dominating, the overestimation of the surface net radiation triggers an overestimation of the evapotranspiration and the previous feedback mechanisms are not in play.

## 4. Future Climate Projections

### 4.1. Sensitivity of the Energy Budget Change to Surface Temperature

To better understand the future temperature changes for scenario RCP8.5, and the related spread among models, we first analyze the future changes of the energy budget, and the corresponding sensitivities to global warming, $S_X(m)$. The regional averages of the sensitivity parameters and the temperature response, together with the intermodel standard deviation are reported in Figure 3a for the five regions. For the four midlatitude regions, the response of $SW_{net}$ radiation is always positive thus increases the energy absorbed by the surface. For CEUR, it is mostly compensated by enhanced cooling by the sensible heat flux. The latent heat flux response is smaller on average across models. It corresponds to a slight decrease in evapotranspiration contributing to heat the surface, with a large spread among models, which is consistent with the transitional nature of the region. By contrast, for CNA, the sensible heat flux response is weak, and the radiation effect is mostly balanced by evaporative cooling, probably because a larger soil moisture allows evapotranspiration to increase with global warming. This is supported by the negative coupling index at the northern frontier and in the western part of the domain indicative of frequent occurrence of energy limited regimes. The sensitivity parameters of SGP and WEAS are between those of CEUR and CNA. For CANA, they are similar to those of CNA, but the strong enhancement of evaporative cooling is mostly compensated by the increase of $LW_{net}$ and $H_s$, in link with the moistening and warming of the boundary layer. The $SW_{net}$ response is smaller on average, with a very large spread, probably related to the regional cloud response to climate change.

Despite different mean behavior in the future change of energy budget, robust conclusions can be drawn on the intermodel spread around the above multimodel mean at the regional scale. We focus on either EF, characterizing the exchange between the land surface and the boundary layer, and SWCRE, indicative of the energy supply to the land surface. Both variables help explaining the magnitude of the warm bias (section 3.2). In the five regions, the spatial averages of the changes in EF and SWCRE are plotted against the corresponding temperature change for each model, together with the corresponding regression lines (Figure 3c). Positive values of the slope correspond to change of $T$ and $X$ that are either both larger or both smaller than model average. Negative values correspond to opposite change of $T$ and $X$ with respect to the model average. Over all regions, models that simulate a higher-than-average warming ($\delta T^a_{i,j}(m) > 0$ in abscissa) are models that also simulate a higher-than-average increase of SWCRE (decrease of its absolute value), resulting in a positive slope of the corresponding (blue) regression line. In regions where the coupling index is positive (SGP, CNA, CEUR, WEAS, and Figures 1c and 3b), the models that warm the most are associated with reduced EF (Figures 3c–3f), consistent with a reduced cooling by evaporation and an increased sensible heat flux (not shown). This link is particularly significant for SGP, CEUR, WEAS, and to a

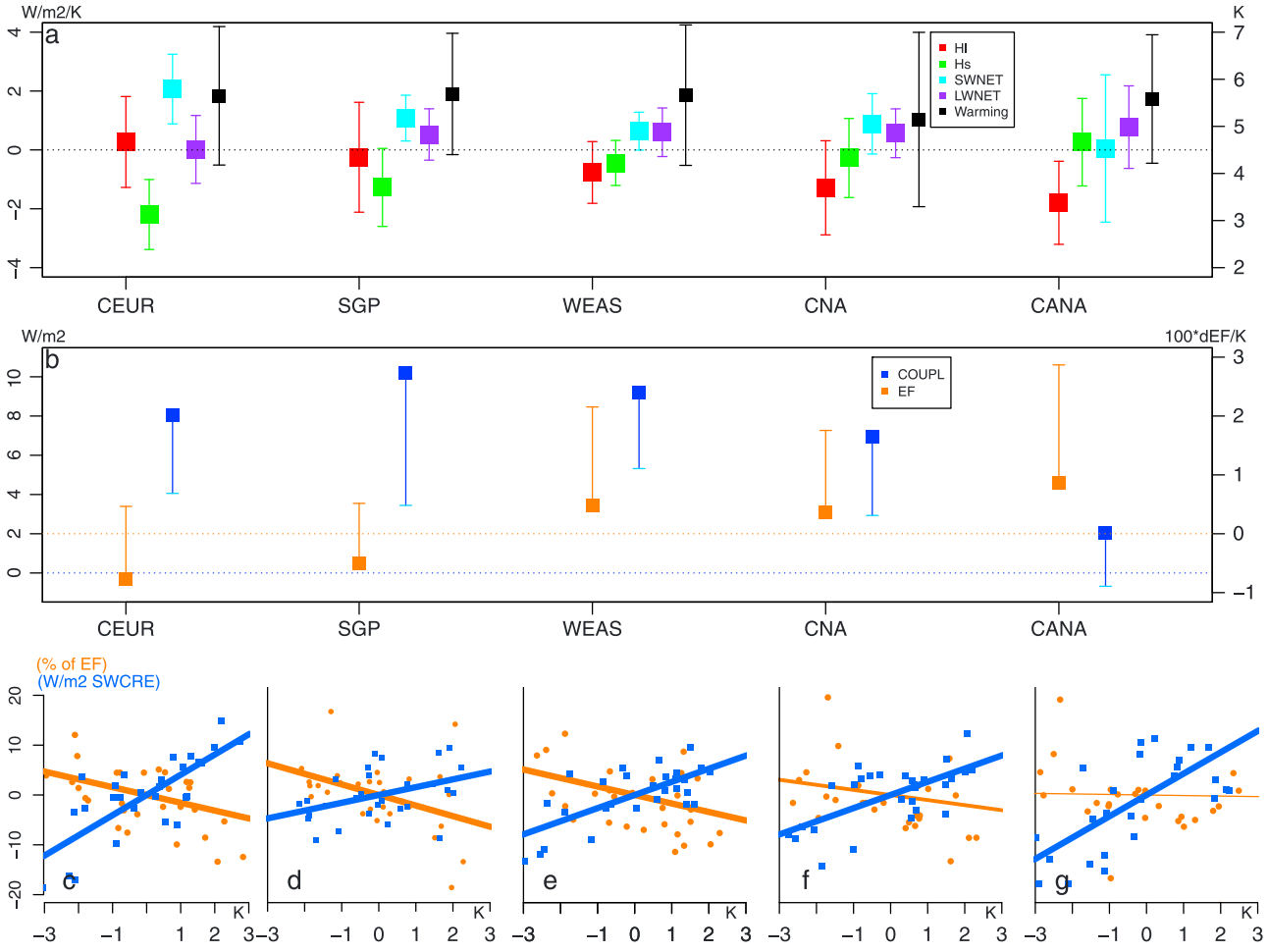


**Figure 3.** Regional analysis in the five boxes of Figure 1: (a) spatial and multimodel means of the local sensitivity parameters $S_X$ (colored squares, unit W m$^{-2}$ K$^{-1}$), and of the local temperature response $\delta T$ (black squares, unit K), together with the multimodel standard deviation of the spatial means; (b) spatial and multimodel means of the present climate coupling index (W m$^{-2}$) and of the local sensitivity parameters for EF (K$^{-1}$); the multimodel standard deviation is only depicted on one side of the multimodel mean, (c–g) relationships between the spatial means of $\delta T^a_{i,j}(m)$ ($x$ axis, unit K) and $\delta X^a_{i,j}(m)$ for EF and SWCRE ($y$ axis, unit W m$^{-2}$ or unitless). The regression lines across models are also displayed, with thick, medium, and thin lines, for $p$ values $< 0.1$, in [0.1, 0.3], and $> 0.3$, respectively. The correlations are the same as between $\delta T_{i,j}(m)$ and $\delta X_{i,j}(m)$, but the regressions lines are centered here on (0, 0), which corresponds to the multimodel mean changes of Figure 3a.

lesser extent for CNA, where the present climate coupling index is lower. These behaviors are consistent with the results of the Global Land-Atmosphere Coupling Experiment CMIP5 (GLACE-CMIP5) multimodel experiment [*Seneviratne et al.*, 2013], where climate models were integrated with and without interactive soil moisture, and which shows that the temperature differences between the two experiments scale with the latent heat differences. For the CANA region, where energy-limited regimes are likely to dominate, and the averaged coupling index is low or even negative, the intermodel spread in the warming is not linked with the spread in the EF response to global warming.

These results are confirmed when considering the intermodel correlation coefficients between the global warming response of EF or of SWCRE (Figures 1g–1h), and the RCP8.5 temperature change. The regional correlation highlights the regions where uncertainties in the response of the clouds and/or surface processes are likely to impact the spread of the temperature projections. Consistently with Figure 3, $\delta$SWCRE is strongly correlated with the projected warming over most land areas. The EF signal is less extended than the SWCRE signal, but over wide areas, including the southern United States, and the western and central part of Europe (to the north of the Alps), there is a significant anticorrelation between $\delta T$ and $\delta$EF (Figure 1g). In these regions, evaporation is primarily limited by the available soil moisture (Figure 1c), suggesting that the spread of soil moisture has a significant impact on the spread of EF response and of the projected

warming. When local warming anomalies ($\delta T^l$) are considered in the correlations with $\delta$EF and $\delta$SWCRE, the correlation is weaker for SWCRE and EF variations (see supporting information). We interpret this as an indication of how much the local processes modulate the climate sensitivity at regional scale (two models with the same global climate sensitivity could have different local climate sensitivities because of local EF and SWCRE controls). For instance, clouds and rain are controlled both by large-scale/global processes (e.g., SST and large-scale circulation) and local processes through the coupling of the boundary layer with the soil processes [*Santanello et al.*, 2011].

### 4.2. Link Between Future Warming Intensity and Present Climate Deficiencies

Figure 1d displays the intermodel correlation coefficients between temperature bias with respect to CRU for the historical simulations ($T^b_{i,j}(m, \exp)$) and the RCP8.5 temperature change $\delta T_{i,j}$. Areas with very positive correlation are found in the midlatitudes, where they largely intersect with the areas of warm bias (Figures 1a and 1b). This means that the areas of largest warming (relatively to the multimodel regional mean) in the midlatitude are the areas of large summer warm bias. Thus, we investigate the possible link between the intensity of regional-scale warming and the values of EF and SWCRE for the present climate (Figures 1e–1f). Like for the warm bias, we find a negative/positive correlation between historical EF/SWCRE values and future warming. For the midlatitude regions, the correlation is significant over most biased areas (Figure 1a), except over CANA for EF and SWCRE, and over WEAS for EF. Moreover, where the correlation is significant, the models simulating the largest warming are associated with the lowest EF and/or the weakest SWCRE in the present climate, as it is the case for the most biased models in SGP, CNA, CEUR, and WEAS (see previous section). The similarity between Figures 1d and 1f gives strong indication that the cloud deficit identified in the present-day simulations for the most biased models in summer and at midlatitude is a very robust source of amplification of the warming. The difficulty of sustaining evaporation reinforces this effect in limited regions as suggested by the more patchy structure of Figure 1e.

## 5. Summary and Conclusions

This work aims at better understanding the spread of the Northern Hemisphere summer temperatures in climate simulations from the CMIP5 database. This quasi-systematic and strong bias should constitute a challenge for the climate modeling community. A warm bias is diagnosed in most models for AMIP simulations. For the historical simulations, produced with coupled ocean-atmosphere models, the patterns of the differences with the observations are similar, although the amplitude of the warm bias is markedly reduced. This bias reduction in coupled simulations (probably for compensation errors) might explain why no more attention has been paid so far to this bias. SWCRE is underestimated where models exhibit a warm bias. In the midlatitudes, the spatial distribution of the mean bias exhibits common features with the one of the soil moisture-atmosphere coupling index in the present climate, which reveals areas where soil moisture supply is the principal control on latent heat flux. In these regions, the net SW radiation is overestimated in links with a cloud deficit which may have local as well as large-scale origins, EF is underestimated as well which may result from the following: (i) the enhancement of evaporative demand by the cloud deficit and (ii) the failure to meet this demand due to either lack of soil moisture or defects of the land surface model. This points two positive feedback mechanisms (excess of net surface radiation supply and insufficient evaporative cooling) to be at play in the midlatitude regions which show a warm bias. The above deficiencies of the present climate simulations impact the future climate projections. Over extended areas, the most biased models in the present climate tend to have a higher sensitivity to climate change. In addition, the models that simulate a higher-than-average warming are models that simulate a larger-than-average $SW_{net}$ increase, in link with a higher-than-average reduction of the screening effect of the clouds. In regions with effective soil moisture-atmosphere coupling, identified by a positive coupling index, the models that warm the most are associated with an higher-than-average decrease of evaporative fraction, due to a lower-than-average cooling by evapotranspiration and an enhanced cooling by the sensible heat flux. This shows that the same feedback mechanisms identified for the warm-biased areas for the present climate are in play for the future climate projections and can artificially amplify the climate warming at regional scale. In boreal areas (e.g., CANA), no impact of the spread of the evaporative fraction response to the global warming on the local warming is found.

There are also some hints of both local sources of climate sensitivity (related to land surface-atmosphere feedback) and global sources (related to cloud and radiative processes), which have to be further explored.

Many other sources of dispersion exist as well, which are overlooked in this study. In particular, a summer soil moisture deficit can originate from a winter precipitation deficit [*Vautard et al.*, 2007]. As the areas with effective soil moisture-atmosphere coupling are expected to expand with climate change [*Dirmeyer et al.*, 2013], it is likely that conditions which generate the warm bias in the present climate expand regionally, which may artificially amplify the climate sensitivity.

**Acknowledgments**

This research was supported by the European Commission's Seventh Framework Programme EMBRACE project (grant 282672). To analyze the CMIP5 data, this study benefited from the IPSL Prodiguer-Ciclad facility which is supported by the L-IPSL project which is funded by the Agence Nationale de la Recherche under the "Programme d'Investissements d'Avenir" (grant ANR-10-LABX-0018) and by the IS-ENES2 project which is funded by the European Commission under the Seventh Framework Programme (grant 312979). We acknowledge F. Wang for the extraction of the latent heat and sensible heat fluxes from the *Jung et al.* [2011] data, the World Climate Research Programme's Working Group on Coupled Modeling, which is responsible for CMIP, and we thank the climate modeling groups (listed in Table S1 of the supporting information) for producing and making available their model output. For CMIP the U.S. Department of Energy's Program for Climate Model Diagnosis and Intercomparison provides coordinating support and led development of software infrastructure in partnership with the Global Organization for Earth System Science Portals.

The Editor thanks two anonymous reviewers for their assistance in evaluating this paper.

## References

Baldocchi, D., et al. (2001), FLUXNET: A new tool to study the temporal and spatial variability of ecosystem-scale carbon dioxide, water vapor, and energy flux densities, *Bull. Am. Meteorol. Soc.*, *82*, 2415–2434, doi:10.1175/1520-0477(2001)082<2415:FANTTS>2.3.CO;2.

Boberg, F., and J. H. Christensen (2012), Overestimation of Mediterranean summer temperature projections due to model deficiencies, *Nat. Clim. Change*, *2*(6), 433–436, doi:10.1038/nclimate1454.

Boé, J. (2013), Modulation of soil moisture/precipitation interactions over France by large scale circulation, *Clim. Dyn.*, *40*, 875–892, doi:10.1007/s00382-012-1380-6.

Boé, J., and L. Terray (2008), Uncertainties in summer evapotranspiration changes over Europe and implications for regional climate change, *Geophys. Res. Lett.*, *35*, L05702, doi:10.1029/2007GL032417.

Campoy, A., A. Ducharne, F. Cheruy, F. Hourdin, J. Polcher, and J. C. Dupont (2013), Response of land surface fluxes and precipitation to different soil bottom hydrological conditions in a general circulation model, *J. Geophys. Res. Atmos.*, *118*, 10,725–10,739, doi:10.1002/jgrd.50627.

Cheruy, F., A. Campoy, J.-C. Dupont, A. Ducharne, F. Hourdin, M. Haeffelin, M. Chiriaco, and A. Idelkadi (2013), Combined influence of atmospheric physics and soil hydrology on the simulated meteorology at the SIRTA atmospheric observatory, *Clim. Dyn.*, *40*, 2251–2269, doi:10.1007/s00382-012-1469-y.

Christensen, J., and F. Boberg (2012), Temperature dependent climate projection deficiencies in CMIP5 models, *Geophys. Res. Lett.*, *39*, L24705, doi:10.1029/2012GL053650.

Coindreau, O., F. Hourdin, M. Haeffelin, A. Mathieu, and C. Rio (2007), Assessment of physical parameterizations using a global climate model with stretchable grid and nudging, *Mon. Weather Rev.*, *135*(4), 1474–1489, doi:10.1175/MWR3338.1.

Coppola, E., et al. (2014), Present and future climatologies in the phase I CREMA experiment, *125*, 23–38, doi:10.1007/s10584-014-1137-9.

Dirmeyer, P. A. (2011), The terrestrial segment of the soil moisture-climate coupling, *Geophys. Res. Lett.*, *38*, L16702, doi:10.1029/2011GL048268.

Dirmeyer, P. A., Y. Jin, and X. Yan (2013), Trends in land-atmosphere interactions from CMIP5 simulations, *J. Hydrometeorol.*, *14*, 829–849, doi:10.1175/JHM-D-12-0107.1.

Fischer, E. M., S. I. Seneviratne, P. L. Vidale, D. Lüthi, and C. Schär (2007), Soil moisture-atmosphere interactions during the 2003 European summer heat wave, *J. Clim.*, *20*, 5081–5099, doi:10.1175/JCLI4288.1.

Giorgi, F., and E. Coppola (2010), Does the model regional bias affect the projected region climate change? An analysis of global model projections, *Clim. Change*, *100*, 787–795, doi:10.1007/s10584-010-9864-z.

Guo, Z., et al. (2006), GLACE: The global land-atmosphere coupling experiment. Part II: Analysis, *J. Hydrometeorol.*, *7*(611–625), doi:10.1175/JHM511.1.

Jaeger, E., and S. I. Seneviratne (2011), Impact of soil moisture atmosphere coupling on European climate extremes and trends in a regional climate model, *Clim. Dyn.*, *36*, 1919–1939.

Jiménez, C., et al. (2011), Global intercomparison of 12 land surface heat flux estimates, *J. Geophys. Res.*, *116*, D02102, doi:10.1029/2010JD014545.

Jung, M., et al. (2011), Global patterns of land-atmosphere fluxes of carbon dioxide, latent heat, and sensible heat derived from eddy covariance, satellite, and meteorological observations, *J. Geophys. Res.*, *116*, G00J07, doi:10.1029/2010JG001566.

Kato, S., N. G. Loeb, F. G. Rose, D. R. Doelling, D. A. Rutan, T. E. Caldwell, L. Yu, and R. A. Weller (2013), Surface irradiances consistent with CERES-derived top-of-atmosphere shortwave and longwave irradiances, *J. Clim.*, *26*, 2719–2740, doi:10.1175/JCLI-D-12-00436.1.

Mitchell, T., and P. Jones (2005), An improved method of constructing a database of monthly climate observations and associated high-resolution grids, *Int. J. Climatol.*, *25*, 693–712, doi:10.1002/joc.1181.

Mueller, B., and S. I. Seneviratne (2014), Systematic land climate and evapotranspiration biases in CMIP5 simulations, *Geophys. Res. Lett.*, *41*, 128–134, doi:10.1002/2013GL058055.

Santanello, J. A. J., C. D. Peters-Lidard, and S. V. Kumar (2011), Diagnosing the sensitivity of local land-atmosphere coupling via the soil moisture-boundary layer interaction, *J. Hydrometeorol.*, 766–786, doi:10.1175/JHM-D-10-05014.1.

Seneviratne, S. I., et al. (2013), Impact of soil moisture-climate feedbacks on CMIP5 projections: First results from the GLACE-CMIP5 experiment, *Geophys. Res. Lett.*, *40*, 5212–5217, doi:10.1002/grl.50956.

Taylor, K., R. J. Stouffer, and G. A. Meehl (2012), An overview of CMIP5 and the experiment design, *Bull. Am. Meteorol. Soc.*, *93*, 485–498, doi:10.1175/BAMS-D-11-00094.1.

Vautard, R., P. Yiou, F. D'Andrea, N. de Noblet, N. Viovy, C. Cassou, J. Polcher, P. Ciais, M. Kageyama, and Y. Fan (2007), Summertime European heat and drought waves induced by wintertime Mediterranean rainfall deficit, *Geophys. Res. Lett.*, *34*, L07711, doi:10.1029/2006GL028001.

Vautard, R., et al. (2013), The simulation of European heat waves from an ensemble of regional climate models within the EURO-CORDEX project, *Clim. Dyn.*, *41*, 2555–2575, doi:10.1007/s00382-013-1714-z.